18

Ferroelectric Optics:Optical Bistability in Nonlinear Kerr Ferroelectric Materials

Abdel-Baset M. A. Ibrahim[1], Mohd Kamil Abd Rahman[1], and Junaidah Osman[2]

[1]*School of Physics and Material Sciences, Faculty of Applied Sciences, Universiti Teknologi MARA, 40450 Shah Alam, Selangor,*

[2]*School of Physics, Universiti Sains Malaysia, 118000 USM, Penang, Malaysia*

1. Introduction

Ferroelectric oxides with perovskite structure such as $PbLaTiO_3$ (PLT), $BaTiO_3$, $PbTiO_3$, $SrBi_2Ta_2O_9$ and $LiNbO_3$ are very attractive class of materials which possess numerous useful properties such as high dielectric constant, large spontaneous polarization, and remarkable optical nonlinearity. Potential applications of these materials include real-time holography, correlation filtering and various novelty filter applications (Sutherland 1996 and Eaton 1991). They are also popular materials for the fabrication of nonvolatile memories (Ramesh 2001). Over the past few years, ferroelectric oxides have been widely investigated for various nonlinear optical applications (Shi 2006; Xuan 1998; Zhang 1999; Zhao 1996) especially for optical switches. Optical switches are devices invented to perform multiplexing at very fast speeds and with less delay than the customary switches works with electronic signals. A ferroelectric optical switch is expected to allow the processing of millions of signals at a speed of terahertz.

To obtain optical bistability phenomenon, two ingredients are necessary, a nonlinear process and a feedback mechanism (Gibbs, 1977, 1979, and 1985). In all optical systems, the feedback can be "distributed", "extrinsic" or "intrinsic". In multilayer systems with alternating nonlinear materials, the feedback is "distributed"; it arises from the interaction of the propagating wave with many cross-sections of a nonlinear medium. In a Fabry-Perot (FP) resonator, the feedback is "extrinsic"; it arises as a result of reflection from the mirrors placed at its interface. In a single nonlinear layer, the feedback can be "intrinsic" or "mirrorless"; it arises in each elementary oscillator due to the strong local nonlinear response of an individual atom or molecule.

In the usual or the standard analysis to study the optical bistability (Marburger 1978, Gupta 1987, Biran 1990, Danckaert 1989, Shen 1984, and Haelterman 1989) in nonlinear optics, the governing equation for optical propagation within the nonlinear medium is a nonlinear wave equation in the electric field derived from Maxwell's equations. The usual constitutive relation between the nonlinear polarization and the electric field is then obtained by expanding the nonlinear polarization as a Taylor series in the electric field. The usefulness of this constitutive relation is that the polarization is a natural source term in the Maxwell's

equation. Even though such constitutive relation is used to describe majority of the nonlinear optical phenomena, it is not essential or unique. Goldstone and Garmire (Goldstone 1984), in their work on the intrinsic bistability in semi-infinite nonlinear medium, used an inverted form of the usual constitutive relation. They expressed the electric field in terms of the total polarization ussing the nonlinear Duffing anharmonic oscillator equation and solved the nonlinear wave equation in terms of polarization as the independent variable. They stressed that the usual analysis in nonlinear optics is not suitable to describe a potentially important class of bistable interactions which result from intrinsic material bistability.

The advantage of Duffing constitutive relation is that the driving field is treated as dependant on the material response which allows to account for the optical bistability results from the intrinsic feedback mechanisim even in microscopic domain. An additional advantage of using the Duffing Oscillator over the usual constitutive relation is that the exact nature of the nonlinear susceptibility $\chi^{(3)}$ of the material is not required because the nonlinearity of the system is automatically contained in the induced polarization (Ibrahim 2007). Moreover if we are dealing with operating wavelength in the neighborhood of resonance where the nonlinear material usually exhibits a huge third order nonlinearity , the usual constitutive relation becomes really questionable since the undepleted wave approximation is clearly violated.

Recently, Murgan *et al*. (2002) have derived expressions of the tensor elements for various second- and third-order nonlinear optical effects including optical Kerr effect for bulk FE materials having various symmetries. They have shown that many of these elements have large linear and nonlinear optical coefficients even in the visible and near-infrared frequency regions. Particularly near resonance, the FE materials becomes highly nonlinear. They have found that it is the combination of the temperature divergence and the resonant frequency, which is typically in the THz region, dependence that underlies their large values. For these reasons, it is believed that the Maxwell-Duffing analysis is more suitable for investigating optical bistability in Kerr FE materials especially when the operating frequency is in the resonance region.

In this chapter, the Maxwell-Duffing approach will be applied to investigate the optical bistability in ferroelectric materials with Kerr nonlinearity. For ferroelectric materials, the Landau-Khalatnikov dynamical equation is used with anharmonic potential as the constitutive relation. Such nonlinear binding potential is provided from the Landau-Devonshire free energy for bulk ferroelectric exhibiting second-order phase transitions. A nonlinear polarization equation is derived and integrated across the ferroelectric medium. Through the application of the exact boundary conditions, expressions for reflectance R, transmittance $\mathbf{T}$, are derived as a function of the polarization P and the driving field $\boldsymbol{E}$. Results for both Fabry-Perot resonators filled with a ferroelectric medium and for a ferroelectric slab without coating mirrors will be presented. The nonlinear response of the polarization, reflectance and transmittance as a function of the electric field incident amplitude will be illustrated. The effect of thickness, operating frequency, and temperature on the bistable characteristics of the FE slab will also demonstrated. In the case of FP resonator with partially reflecting mirrors, the effect of mirror reflectivity on the optical bistability is studied. The possibility of obtaining a reliable optical switch from such system will be explored. The examples shown in this chapter are based on the available experimental data of $BaTiO_3$.

2. Mathematical formulation

Consider a Fabry Pérot resonator filled with bulk ferroelectric crystal and coated with a pair of thin identical partially-reflecting mirrors as illustrated in Fig. 1. A high intensity incident infrared radiation is impinging the material at normal incidence. The nonlinear ferroelectric material ($BaTiO_3$) is assumed in the ferroelectric phase and exhibits a second-order like phase transitions. To derive a nonlinear polarization wave equation for medium 2, we begin by considering Landau-Devonshire free energy F expression written in terms of the polarization $\boldsymbol{P}(z,t)$ as following (Lines and Glass, 1977)

$$F(\boldsymbol{P},T)=\frac{\alpha}{2\varepsilon_0}\boldsymbol{P}^2+\frac{\beta}{4{\varepsilon_0}^2}\boldsymbol{P}^4-\boldsymbol{E}.\boldsymbol{P} \tag{1}$$

The parameter $\alpha=a(T-T_c)$ is temperature-dependent with a being the inverse of the Curie constant, T is the thermodynamic temperature, and T_c is the Curie temperature. The parameter β is the nonlinear coefficient; it is material-dependent with mechanical dimension m^3J^{-1} and ε_0 is the dielectric permittivity of vacuum. The term $\boldsymbol{E}.\boldsymbol{P}$ accounts for the coupling of the far infra-red (FIR) radiation with the driving field $\boldsymbol{E}$. The response of a FE material exposed may be described by the time-dependent Landau-Khalatnikov dynamical equation of motion in terms of polarization, $\boldsymbol{P}$, as

$$M\frac{d^2\boldsymbol{P}}{dt^2}+\Gamma\frac{d\boldsymbol{P}}{dt}=-\frac{\partial F}{\partial \boldsymbol{P}} \tag{2}$$

In the above, M is the inertial coefficient with mechanical dimension $Kg.m^3A^{-2}.s^{-2}$. The term $\Gamma d\boldsymbol{P}/dt$ represents the linear loss and Γ is a damping parameter with mechanical dimension $Kg.m^3.A^{-2}.s^{-3}$. The driving field $\boldsymbol{E}$ in the FE medium is considered to have a form of uniform time-harmonic plane wave propagating in the negative z-direction at fundamental frequency ω

$$\boldsymbol{E}_2(z,t)=\frac{1}{2}\left[E_2(z)\exp(-i\omega t)+E_2^*(z)\exp(+i\omega t)\right] \tag{3}$$

In equation (3), $E_2(z)$ and $E_2^*(z)$ are the electric field amplitude in the ferroelectric medium and it complex conjugate respectively. The total polarization $\boldsymbol{P}(z,t)$ is also considered to be time harmonic, in phase, and propagates in same direction as the $\boldsymbol{E}$ field, which is

$$\boldsymbol{P}(z,t)=\frac{1}{2}\left[P(z)\exp(-i\omega t)+P^*(z)\exp(+i\omega t)\right] \tag{4}$$

In equation (4), $P(z)$ and $P^*(z)$ are the polarization amplitude and its complex conjugate respectively. Therefore, substituting (1), (3) and (4) into (2) gives the following time-independent Landau-Khalatnekov equation

$$E_2(z)=\left[-M\omega^2-i\Gamma\omega+a(T-T_c)/\varepsilon_0\right]P(z)+\left(3\beta/4{\varepsilon_0}^2\right)\left|P(z)\right|^2P(z) \tag{5}$$

Equation (5) is the time-independent form of equation (2); it describes the electric field in the ferroelectric medium in terms of polarization and other material parameters. In deriving equation (5), the third-harmonic term is usually ignored. The corresponding magnetic field is derived from equation (5) using the relation $H_{2,x}(z)=\left(i/\omega\mu_0\right)\left(dE_{2,y}/dz\right)$, where here for simplicity we have considered E_2 to be purely polarized in the *y*-direction $\left(0,E_y,0\right)$, and H is purely polarized in the *x*-direction $\left(H_x,0,0\right)$. Therefore,

$$H_{2,x}(z)=\frac{i}{\omega\mu_0}\frac{3\sqrt{3}}{8}\left\{4\left[-M\omega^2-i\Gamma\omega+a\left(T-T_c\right)/\varepsilon_0\right]\frac{dP(z)}{dz}+\frac{\beta}{{\varepsilon_0}^2}\left[3P^2(z)\frac{dP^*(z)}{dz}+6\left|P(z)\right|^2\frac{dP(z)}{dz}\right]\right\} \tag{6}$$

In linear régime $\left(\beta=0\right)$, equation (5) may be combined with the linear equation $P=\varepsilon_0\chi(\omega)E$ to obtain the linear dielectric function $\varepsilon(\omega)$ for ferroelectric medium

$$\varepsilon(\omega)=\varepsilon_\infty+\left[-M\omega^2-i\Gamma\omega+a\left(T-T_c\right)/\varepsilon_0\right]^{-1} \tag{7}$$

From equation (7), the linear refractive index of the FE medium may be evaluated as $n_2=\left[\varepsilon(\omega)\right]^{1/2}$. ε_∞ is the high-frequency limit of the dielectric function $\varepsilon(\omega)$. Equation (7) is essentially similar to that of typical dielectric except that it is temperature-dependent function. For convenience in the numerical work, it is helpful to scale the relevant equations and use dimensionless variables (Lines and Glass 1977). Therefore the dimensionless parameters are being introduced;

$$e_2=E_2/E_c,\quad f=\omega/\omega_0,\quad p=P/P_s,\quad t=T/T_c,\quad u=\omega_0 z/c \tag{8}$$

Equation (8) shows that the coercive field of ferroelectric material at zero temperature E_c is used to scale the dimensional electric field inside the FE medium to give the scaled electric field e_2. In similar fashion, the resonance frequency ω_0 is used to scale the operating frequency ω to give a scaled operating frequency *f*. The polarization *P* and the thermodynamic temperature *T* are scaled in terms of spontaneous polarization at zero temperature P_s and the Curie temperature T_c respectively. Finally, the thickness *z* is scaled by dividing out c/ω_0 to give a scaled thickness $u=\omega_0 z/c$. In fact, any physical variable can be made dimensionless just by dividing out a constant with similar dimension. For helpful discussion about scaling analysis of physical equations, the reader is referred to Snieder (2004). Therefore, substituting the scaled parameters of equation (8) into equation (5), we obtain the following dimensionless form of Landau-Khalatnikov equation;

$$e_2=\frac{3\sqrt{3}}{8}\left[4\left(t-1-mf^2-ifg_F\right)+3\left|p(u)\right|^2\right]p(u) \tag{9}$$

In equation (9), the coefficient $m=\left[M\omega_0^2\varepsilon_0/aT_c\right]$ is the scaled inertial coefficient while $g_F=\left[\Gamma\omega_0\varepsilon_0/aT_c\right]$ is the scaled damping parameter. To describe the propagation in the ferroelectric medium, the time-independent electromagnetic wave equation $d^2E_2/dz^2+\left(\omega^2\varepsilon_\infty/c^2\right)E_2+\omega^2\mu_0P=0$ is employed. However, this equation has to be converted to

dimensionless form using the scaled parameters in equation (8) as well. This yields the following scaled form of the electromagnetic wave equation;

$$\frac{d^2 e_2}{du^2} + f^2 \varepsilon_\infty e_2 + f^2 \frac{P_0}{E_0 \varepsilon_0} p(u) = 0 \tag{10}$$

Substituting the electric field expression from equation (9) into the wave equation (10), the following nonlinear polarization equation is obtained;

$$2\left[2\hbar + 3|p|^2\right]\frac{d^2 p}{du^2} + 3p^2 \frac{d^2 p^*}{du^2} + 12p\frac{dp}{du}\frac{dp^*}{du} + 6p^*\left[\frac{dp}{du}\right]^2 + f^2\varepsilon_\infty\left[4\left(\hbar + \xi\right) + 3|p|^2\right]p = 0 \tag{11}$$

Equation (11) is a nonlinear equation describes the evolution of the polarization in a ferroelectric medium with thickness *u*. For simplicity, we have introduced the scaled coefficients ξ and $\hbar$ in equation (11), where $\xi = \left(2\sqrt{3}/9\right)\left(P_s / E_c \varepsilon_0 \varepsilon_\infty\right)$ and $\hbar = t - 1 - mf^2 - ifg_F$. For ferroelectric material exhibits a second-order phase transitions, the coercive field at zero temperature is $E_c = +\sqrt{4a^3 T_c^3 / 27\varepsilon_0 \beta}$ while the spontaneous polarization at zero temperature is $P_s = \sqrt{aT_c \varepsilon_0 / \beta}$. Upon substituting the value of P_s and E_c, the value of ξ reduces to $\xi = \left(\varepsilon_\infty a T_c\right)^{-1}$ which is basically a constant value for each specific material. The coefficient $\hbar$ is also important since it contains contributions from thermodynamic temperature *t*, operating frequency *f*, and the damping parameter g_F.

To obtain numerical solution, it is helpful to eliminate the term $d^2 p^* / du^2$ from equation (11). This can be done as follows; first, the complex conjugate of equation (11) is obtained. Second, the term $d^2 p^* / du^2$ is eliminated between equation (11) and its complex conjugate. This leads to the following nonlinear propagation equation,

$$\begin{aligned}&\left[16|\hbar|^2 + 24\left(\hbar + \hbar^*\right)|p|^2 + 27|p|^4\right]\frac{d^2 p}{du^2} + 12\left(2\hbar^* + 3|p|^2\right)p^*\left[\frac{dp}{du}\right]^2 - 18p^3\left[\frac{dp^*}{du}\right]^2 \\ &+12\left(4\hbar^* + 3|p|^2\right)p\frac{dp}{du}\frac{dp^*}{du} + f^2\varepsilon_\infty p\left[16\hbar^*\left(\hbar + \xi\right) + 12\left(2\hbar + \xi\right)|p|^2 + 9|p|^4\right] = 0\end{aligned} \tag{12}$$

In equation (12), the coefficient $\hbar^* = t - 1 - mf^2 + ifg_F$ is the complex conjugate of $\hbar$. Equation (12) may be integrated numerically across the ferroelectric medium as an initial value problem to evaluate the desired polarization.

3. Analysis of the Fabry-Perot Interferometer

The analysis to find the complex reflection *r*, and transmission coefficients τ, is basically similar to the standard analysis in linear optics (Born & Wolf 1980); where $\boldsymbol{R} = |r|^2$ and $\boldsymbol{T} = |\tau|^2$ represent the reflected and transmitted intensities respectively. Referring to Fig. 1, the electric fields in medium1 and 3 are assumed to have the form of a plane wave propagating in free space with propagation constants $k_1 = k_3 = k_0 = \omega n_0 / c$ and $n_0 = 1$. Therefore, we may write

$$E_1 = E_0\left[\exp(-ik_1 z) + r\exp(ik_1 z)\right] \tag{13}$$

$$H_1 = \left(E_0 k_1/\omega\mu_0\right)\left[\exp(-ik_1 z) - r\,\exp(ik_1 z)\right] \tag{14}$$

$$E_3 = \tau E_0 \exp\left[-ik_3\left(z+L\right)\right] \tag{15}$$

$$H_3 = k_3\left(E_0/\omega\mu_0\right)\tau\exp\left[-ik_3\left(z+L\right)\right] \tag{16}$$

where, E_0 is the amplitude of the incident electric field. At top interface, The tangential components of the electric field E is continuous with $E_1^{\parallel}(z=0) = E_2^{\parallel}(z=0)$ where E_1 and E_2 are substituted from equation (13) equation (5) respectively. The standard scaling procedure then yields the following expression for complex reflection coefficient r;

$$r = \frac{3\sqrt{3}}{8e_0}\left[4\hbar p_t(u) + 3p_t(u)\left|p_t(u)\right|^2\right] - 1 \tag{17}$$

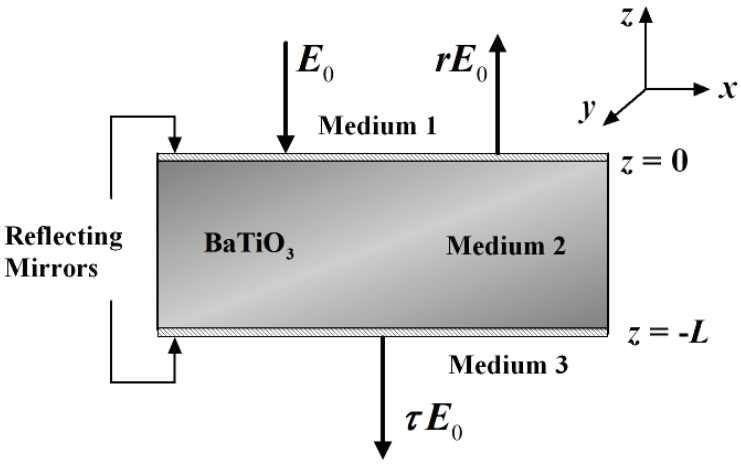

Fig. 5.1. Geometry of the Fabry-Pérot resonator.

The subscript t of p_t in equation (17) refers to the polarization at top interface. Due to the existence of the mirrors at both interfaces , the boundary conditions for the magnetic field at top interface becomes $H_{1x}(z) - \eta E_{1y}(z) = H_{2x}(z)$ (Lim, 1997) where H_{1x}, E_{1y}, and H_{2x} are represented by equations (6), (13), and (14) respectively. The parameter $\eta = \eta_a - i\eta_b = \sigma_M\delta_M - i\omega\varepsilon_0\varepsilon_M\delta_M$ is the mirror coefficient with conductivity σ_M, thickness δ_M, and permittivity of the mirror medium ε_M respectively. For perfect dielectric mirror with conductivity $\sigma_M \to 0$ the term η_a becomes zero. In such a case the wave propagates into the mirror material without attenuation. Experimentally such coating mirror can be designed to meet the required reflectance at optimized wavelength using various metallic or dielectric materials. The standard scaling procedure, then yields following dimensionless equation for the magnetic field at top interface;

$$\left[(1-r)+(1+r)\eta_s\right]fe_0 = i\frac{27}{4}\left[\hbar + i\frac{3}{2}\left|p_t\right|^2\right]\frac{dp_t}{du} + i\frac{81}{16}p_t^2\frac{dp_t^*}{du} \tag{18}$$

In equation (18), $\eta_s = c\mu_0\eta = \eta_{s,a} - i\eta_{s,b}$ accounts for the scaled mirror parameter and for purly dielectric mirror $\eta_{s,a} = 0$ and η_s reduces to $-i\eta_{s,b}$. If we eliminate the complex reflection coefficient *r* between equations (17) and (18), the following equation is obtained;

$$e_0 = \frac{3}{16f}\left\{\sqrt{3}\left(1-\eta_s\right) f\left[4\hbar p_t + 3\left|p_t\right|^2 p_t\right] + 9i\left[2\left(2\hbar + 3\left|p_t\right|^2\right)\frac{dp_t}{du} + 3{p_t}^2\frac{dp_t^*}{du}\right]\right\} \tag{19}$$

Equation (19) will be used later to evaluate the amplitude of incident electric field e_0 numerically as a function the polarization at top interface. In similar fashion, the boundary conditions at the bottom boundary $z = -L$ are applied. Continuation of the tangential components of E at $z = -L$ $\left(E_2^{\parallel} = E_3^{\parallel}\right)$ yields an expression for the complex transmission coefficient;

$$\tau = \frac{3\sqrt{3}}{8e_0}\left[4\hbar + 3\left|p_b\left(u\right)\right|^2\right] p_b\left(u\right) \tag{20}$$

In the above, the subscript *b* in the polarization p_b refers to the bottom boundary. On the other hand, the boundary conditions for the *H*-field $\left(H_{3x} + \eta E_{3y} = H_{2x}\right)$ are also applied where H_{2x} , E_{3y} , and H_{3x} are represented by equations (6), (15), and (16) respectively. The standard scaling procedure, then yields the following dimensionless equation

$$\tau f e_0\left(1+\eta_s\right) = i\frac{27}{4}\left[\hbar + \frac{3}{2}\left|p_b\right|^2\right]\frac{dp_b}{du} + i\frac{81}{16}p_b^2\frac{dp_b^*}{du} \tag{21}$$

Substituting the complex transmission coefficient τ from equation (20) into equation (21), and then eliminating the derivative dp_b^*/du from the resultant equation, the following equation is obtained;

$$\frac{dp_b}{du} = \frac{-i\frac{\sqrt{3}}{9} f p_b\left[6\left(1-\eta_s^*\right)\left(4\hbar^* + 3\left|p_b\right|^2\right)\left|p_b\right|^2 + 4\left(1-\eta_s\right)\left(2\hbar^* + 3\left|p_b\right|^2\right)\left(4\hbar + 3\left|p_b\right|^2\right)\right]}{\left[4\left(2\hbar + 3\left|p_b\right|^2\right)\left(2\hbar^* + 3\left|p_b\right|^2\right) - 9\left|p_b\right|^4\right]} \tag{22}$$

In the former equation, the coefficient $\hbar^*$ and η_s^* are the complex conjugates of $\hbar$ and η_s respectively. Equation (22) is used to evaluate the derivative dp_u/du for arbitrary values of p_b at the bottom interface *z* = -*L*. Both p_b and dp_b/du are used as initial conditions to integrate equation (12) across the ferroelectric medium. . It should be noted that the top boundary *z* = 0 is *u* = 0 in the scaled unit while the bottom boundary *z* = -*L* is *u* = -*l* where $u = \omega_0 z/c$ and $l = \omega_0 L/c$.

4. Intrinsic optical bistability in ferroelectrics

Recently, experimental results concerning intrinsic optical bistability in a thin layer of $BaTiO_3$ monocrystal were presented (Ciolek in 2006). The intrinsic optical bistability in the $BaTiO_3$ monocrystal was achieved through the interaction of two lasers without the application of any optical resonator or external feedback. Further, experimental results

concerning optical bistability of polarization state of a laser beam, induced by the optical Kerr effect of the B_5NH_4 monocrystal was recently observed (Osuch 2004). The measurements were performed by the means of an ellipsometer of a special construction, which allows for the simultaneous measurement of all four polarization parameters of the laser light beam. Other examples of experimentally demonstrated intrinsic optical bistability with different setups of laser sources and geometries of samples have been reported (Hehlen 1994, Pura 1998, Hehlen 1999 & Przedmojski 1978). Therefore, it is equally important to investigate the intrinsic as well as extrinsic optical bistability in FE material and here comes the advantage of Maxwell-Duffing approach over the standard approach. Mathematically, for FE slab without partially reflecting mirrors, the mirror parameter is set to zero $(\eta_s = 0)$ in the relevant equations. Therefore, we will show graphical results of polarization, reflectance, and transmittance versus the electric field input intensity for FE slab as well as for FP resonator.

5. Material aspects

Generally speaking, the mathematical formulation presented here to investigate the optical bistability is valid for any ferroelectric insulating crystal. Particularly, ferroelectrics with high Kerr nonlinearity and photorefractivity. However, in order to obtain more realistic results, material parameters used in simulation are based on published data of $BaTiO_3$. We should point out that below the Curie temperature T_c, all $BaTiO_3$ phase transitions are of the first-order type except that the transition from the cubic to tetragonal phase is a first-order transition close to second-order transitions. Therefore, close to T_c the 6th order term has to be added to the free energy F in equation (1) apart from the type of the transition since at T_c the coefficient β is zero (Ginzburg 2005). However, well below the transition temperature ($T < T_c$) the form provided in equation (1) may be used as an approximation provided that only tetragonal symmetry is considered.

To integrate equation (12) numerically, it is necessary to evaluate certain material-dependent parameters such as $m = \left[M\omega_0^2 \varepsilon_0 / aT_c \right]$, damping coefficient $g_F = \left[\Gamma \omega_0 \varepsilon_0 / aT_c \right]$, and the coefficient $\xi = \left(\varepsilon_\infty aT_c \right)^{-1}$. To determine these scaled parameters, it is necessary to know the dimensional parameters for $BaTiO_3$ such as Curie temperature T_c, the inverse of the Curie constant a, resonance ω_0, and ε_∞. The value of T_c for $BaTiO_3$ used here is $120\ ^oC$ which gives $T_c = 393.15\ K$. We note that, some ferroelectric literature show different values of T_c which slightly differ from $120\ ^oC$. However, $BaTiO_3$ single crystals obtained are usually not so pure because they are grown by the flux method which makes their Curie point usually about $120\ ^oC$ (Mitsui 1976).

The inverse of the Curie constant a is $1/C$ where $C = 1.7 \times 10^5\ K$ (Mitsui 1976). It should be noted that, several ferroelectric books uses the free energy density F in CGS units where $a = 4\pi / C$ $^oC^{-1}$. For example, as in Fatuzzo (1967), the a parameter becomes $a = 4\pi / C = 7.4 \times 10^{-5}\ ^oC^{-1}$. Here, the SI units of measurements are adopted for all dimensional physical variables. It should also be noted that other values of the Curie constant C (Within the range $0.8 \times 10^4 - 1.7 \times 10^5$) have been reported which differs considerably. It seems that the method of preparation and the electronic conductivity of the samples have great influence on the Curie constant. For further details, the reader is referred to Seitz (1957). To estimate the resonance ω_0 for $BaTiO_3$, we use the temperature-dependent relation $\omega_0 = \left[-2a\left(T - T_c\right) / \varepsilon_0 M \right]^{1/2}$ for FE material exhibiting a second-order phase

transitions. Knowing the value of M for BaTiO3 to be 6.44×10^{-21} JmA^{-2} (Murgan 2004), ω_0 is found to be $\omega_0 = 1.437\times10^{13}\left(T_c - T\right)^{1/2}$. At room temperature, ω_0 becomes $\approx 1.43\times10^{14}$ Hz. Other fixed material parameters are damping parameter $\Gamma = 3.32\times10^{-5}$ Kg.m^3.A^{-2}.s^{-3} (Murgan 2004), and the high frequency limit of the dielectric function $\varepsilon_\infty = 3.84$ (Dawber 2005). With these values for the dimensional parameters a, T_c, ω_0, Γ, and ε_∞, the scaled input parameters like m, g and ξ may be calculated.

Since the dimensional polarization amplitude P is scaled in terms of the spontaneous polarization P_s at zero temperature. Therefore, the value of P_s at zero temperature is required. An early measurement of spontaneous polarization P_s by Merz (1949) shows $P_s \approx 0.16$ C.m^{-2} at room temperature then the value drops to $P_s \approx 0.1$ C.m^{-2} at zero temperature. However, here we will consider the value of P_s at zero temperature based on a later measurement on a very good $BaTiO_3$ crystal by Kanzig (1949) and confirmed by Merz in (1953). The later experiment shows a value of P_s = 0.26 C.m^{-2} at room temperature, then it drops to $P_s \approx 0.22$ C.m^{-2} at zero temperature. The discrepancies between the earlier and the later measurements of P_s were attributed to domains which can not be reversed easily (Seitz 1957). The spontaneous polarization curve P_s as a function of temperature (-140 ^{o}C - 120 ^{o}C) obtained by Merz (1953) for $BaTiO_3$ may be also found in various FE books such as Cao (2004) and Rabe (2007).

Because both the dimensional electric field amplitude inside the FE medium E_2 and the incident electric field amplitude E_0 are scaled in terms of the coercive field at zero temperature. Therefore, the value of E_c at zero temperature is also required. First, we discuss the estimated value of E_c using thermodynamic theory and its agreement with the experimentally observed value for $BaTiO_3$. It is possible to estimate the value of E_c using the relation $E_c = +\sqrt{4a^3T_c^3/27\varepsilon_0\beta}$ once the value of the nonlinear coefficient β is known. To do so, we may use the relation $P_s^2 = a\varepsilon_0\left(T_c - T\right)/\beta$ which yields $\beta = \varepsilon_0 a\left(T_c - T\right)/P_s^2$. Substituting the value of $P_s \approx 0.22$ C.m^{-2} at zero temperature (Merz 1953), this yields $\beta \approx 1.3\times10^{-13}$ m^{3}J^{-1}. Therefore, the value of the coercive field is estimated to be $E_c \approx 4\times10^7$ Vm^{-1} at zero temperature. It is important to note that the value of β obtained here is not comparable with those provided by Fatuzzo (1976) and Mitsui (1976) due to the difference in the system of units. In fact their free energy coefficients have different dimensions based on the CGS system of units. However, the value of β obtained here is comparable with that of Murgan (2002) who estimated the value of β to be $\approx 1.9\times10^{-13}$ m^{3}J^{-1} at room temperature based on a value of P_s = 0.1945 C.m^{-2} and $C = 1.669\times10^5$ ***K***. The small difference between the value of β obtained here and that of Murgan (2002) is due to the difference in the value of the spontaneous polarization P_s and thermodynamic temperature.

The theoretical value of the coercive field value $E_c \approx 4\times10^7$ Vm^{-1} calculated at zero temperature using the formula $E_c = +\sqrt{4a^3T_c^3/27\varepsilon_0\beta}$ is in good agreement with other theoretical values calculated elsewhere. For example, a theoretical value of $E_c \approx 1.5\times10^7$ Vm^{-1} for bulk $BaTiO_3$ was mentioned by Mantese (2005). However, the theoretical value of E_c predicted by thermodynamic theory is found to be two orders of magnitude larger than the experimentally observed value (Seitz 1957). For example, an experimental value of $E_c = 3.34\times10^5$ Vm^{-1} for BatTiO3 at room temperature was mentioned by Feng (2002). Here, we use $E_c = 1.2\times10^5$ Vm^{-1} for bulk $BaTiO_3$ at zero temperature based on the measurements by Merz (1953) which is more familiar in ferroelectric literature.

6. Numerical procedure

In linear régime, reflectance **R** and transmittance **T** are independent of the electric field input intensity E_0 and the usual results presented in linear optics are **R** and **T** versus the scaled thickness $l = \omega_0 L/c$. However, in nonlinear optics, as seen from equations (17) and (20), **R** and **T** are directly dependent on the electric field incident amplitude e_0 , and other material parameters such as temperature and thickness. Nonlinear optics text books usually illustrate the optical bistability by showing **T** versus $|e_0|^2$ for fixed value of thickness L and frequency ω . Therefore, our aim here is to generate graphs of this type within our current formalism. Since there is no incoming wave in medium 3, it is more convenient to integrate equation (12) across the FE medium from the bottom interface at $u = -l = -\omega_0 L/c$ to the top interface at $u = \omega_0 z/c = 0$.

Our numerical strategy is basically similar to the computation presented in chapter three which can be summarized as follows: we assume the polarization at the bottom boundary p_b to take an arbitrary real value $(p_b = p_b^*)$ and evaluate the first derivative dp_b/du from equation (22). The choice p_b to be real rather than complex is justified in the work by Chew (2001). We then integrate equation (12) as an initial value problem from the bottom boundary $u = -l$ to the top boundary $u = 0$. The integration process keep tracks of the polarization and its derivative across the medium up to the top boundary $u = 0$. As a result, for each arbitrary value of p_b at bottom boundary, we obtain the corresponding value of the polarization at top boundary p_t , its complex conjugate p_t^* , its first derivative dp_t/du and its first-derivative complex conjugate dp_t^*/du . For certain input parameters, substituting p_t , p_t^* , dp_t/du , and dp_t^*/du into equation (19), we obtain the corresponding value of electric field incident amplitude e_0 . Similarly, the reflectance $\boldsymbol{R} = |r|^2$ is obtained by substituting p_t and p_t^* into equation (17). On the other hand, we evaluate the transmittance $\boldsymbol{T} = |\tau|^2$ at bottom boundary by substituting the polarization at bottom boundary p_b and its complex conjugate p_b^* into equation (20). The integration procedure is then repeated for a large number of arbitrary p_b values and for each time we evaluate e_0 , **R**, and **T.**

Similar numerical scheme to integrate a nonlinear dielectric FP resonator is used by Chew (2001) to evaluate the transmittance of dielectric FP resonator. However, Chew (2001) have generated their plots based on a fixed-step 4th order Runge-Kutta solver modified for complex variable. They therefore, had to perform an interpolation and curve fitting to a raw set of points in the $T - |e_0|$ plane to obtain the optical bistability curves. Here, we have found that the explicit Runge-Kutta method with variable-step solver (Dormand 1980) is capable of producing more accurate results and therefore, an interpolation or any curve fitting is not required and the Bistability curves are generated naturally.

7. Effect of mirror reflectivity

To make a physical significance of the mirror parameter η_s that appeares as a result of the existance of partially reflecting mirrors at the interfaces of the Fabry-Perot resonator, it is useful to to find the corresponding mirror reflectivity R_M of each value of η_s . To do so, we use $R_M = \rho_{j+1,j}\rho_{j+1,j}^*$ where $\rho_{j+1,j} = \left[k_{j+1} - k_j - \eta\right] / \left[k_j + k_{j+1} + \eta\right]$ (Lim 1997) is the elementary reflection coefficient off medium $j+1$ to medium j . k_j and k_{j+1} are the wavenumbers of medium j and medium j+1 respectively. The coeffecient $\rho_{j+1,j}^*$ is the complex conjugate of $\rho_{j+1,j}$ and η accounts for the mirror contribution. In fact, R_M gives the reflectivity of a

mirror placed at the interface of a medium in linear regeme. If both media are nonabsorbing dielectric with $k = \omega n/c$, the coefficient $\rho_{j+1,j}$ may be written in terms of refractive index n and a scaled mirror parameter η_s as $\rho_{j+1,j} = [n_{j+1} - n_j - \eta_s]/[n_j + n_{j+1} + \eta_s]$. If a perfect dielectric nondispersive mirror with conductivity $\sigma_M = 0$ is considered, the mirror coefficient η_s reduces to $-i\eta_{s,b}$ and the mirror reflectivity R_M becomes;

$$R_M = \left[\left(n_{j+1} - n_j \right)^2 + \eta_{s,b}^2 \right] \Big/ \left[\left(n_{j+1} + n_j \right)^2 + \eta_{s,b}^2 \right] \tag{23}$$

For convenience in numerical simulation, it is simpler to consider R_M assuming a range of values between 0 and 1, and then evaluating the corresponding mirror parameter $\eta_{s,b}$ using equation (23).

Fig. 2 shows the mirror parameter $\eta_{s,b}$ versus power reflectivity of the coating mirror R_M based on equation (23). Here, the linear refractive index $n_2 = [\varepsilon(\omega)]^{1/2}$ of the ferroelectric medium calculated using equation (7) is $n_2 \approx 2$ at frequency $f = \omega/\omega_0 = 1.1$. The curve shows that at $\eta_{s,b} = 0$, the reflectivity of the surface is $R \approx 0.11$ and he mirror reflectivity R_M increases gradually with increasing the mirror parameter $\eta_{s,b}$. The corresponding value of R_M is then found for each value of $\eta_{s,b}$ using Fig. 2. To examine the effect of the mirror parameters $\eta_{s,b}$ on the propagation of the polarization wave, we may use equation (12) to plot $|p|$ versus l for different values of $\eta_{s,b}$ (Fig. 3). The solid curve in Fig. 3 shows $|p|$ versus l for $\eta_{s,b} = 0$ (corresponding to $R \approx 0.11$), the dashed curve is for $\eta_{s,b} = 2$ (corresponding to $R_M = 0.38$), the dotted curve for $\eta_{s,b} = 5$ (corresponding to $R_M = 0.76$), and finally the thin-solid curve for $\eta_{s,b} = 10$ (corresponding to $R_M = 0.92$). A comparison between these curves shows a significant increment of the polarization amplitude $|p|$ accompanied by a phase shift which becomes more noticeable with increasing mirror reflectivity R_M. Such increment in the wave amplitude and the corresponding phase change may be due to the constructive interference that gradually builds up as the result of the mirror coating. A highly reflecting mirror plays an important role in improving the bistable performance of a FP resonator particularly it improves its threshold value of bistable operation as will be explained in the upcoming graphs.

As explained in the previous section, the integration of equation (12) as initial value problem together with the boundary conditions allows us to determine the polarization at top and bottom boundary. Further, the electric field incident amplitude is also determined using equation (19). Therefore, we are able to plot the polarization at each boundary as a function of the electric field incident amplitude. To plot the reflectance **R** = $|r|^2$ versus electric field incident amplitude $|e_0|$, both equation (17) and equation (19) are used. Finally, to plot the transmittance **T** = $|\tau|^2$, versus $|e_0|$, both equation (20) and equation (19) are used.

In Figs. 4 we present the optical bistability of a Fabry-Perot resonator coated with an identical pair of partially reflecting dielectric mirrors. The effect of mirror parameter $\eta_{s,b}$ (mirror reflectivity R_M) on the optical bistability is is investigated for various system variables namely, the polarization p, the reflectance **R** and the transmittance **T**. In each graph of Figs. 4 family, the curves are generatd for various mirror parameters ($\eta_{s,b}$ = 0, 0.1, 0.2, 0.5 and 1, which correspond to R_M = 0.11, 0.128, 0.13, 0.15 and 0.2 respectively) while other parameters are fixed at frequency f = 1.1, thickness l = 1.9, $\varepsilon_\infty = 3.84$, resonance $\omega_0 = 1.4 \times 10^{14}$ Hz (evaluated at room temperature). The graphs in general feature typical

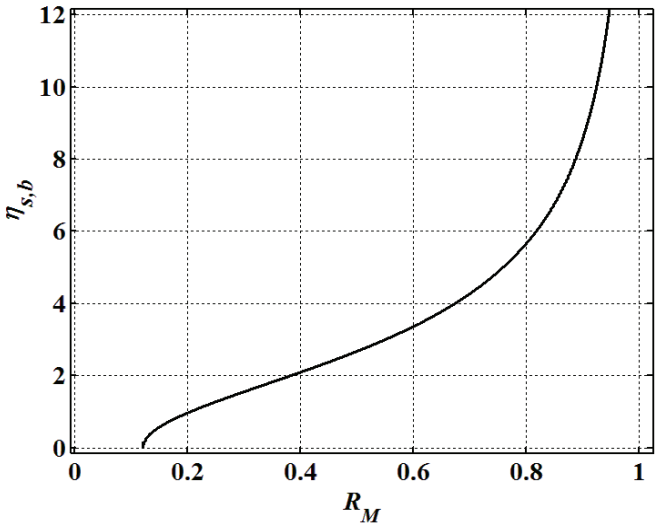

Fig. 2. Scaled mirror parameter $\eta_{s,b} = [\varepsilon_M \delta_M \omega / c]$ versus mirror reflectivity $R_M = \rho_{21}\rho_{21}^*$ placed at single interface between 2 media for scaled frequency f = 1.1, linear refractive index $n_2 = 2$ and $n_1 = 1$.

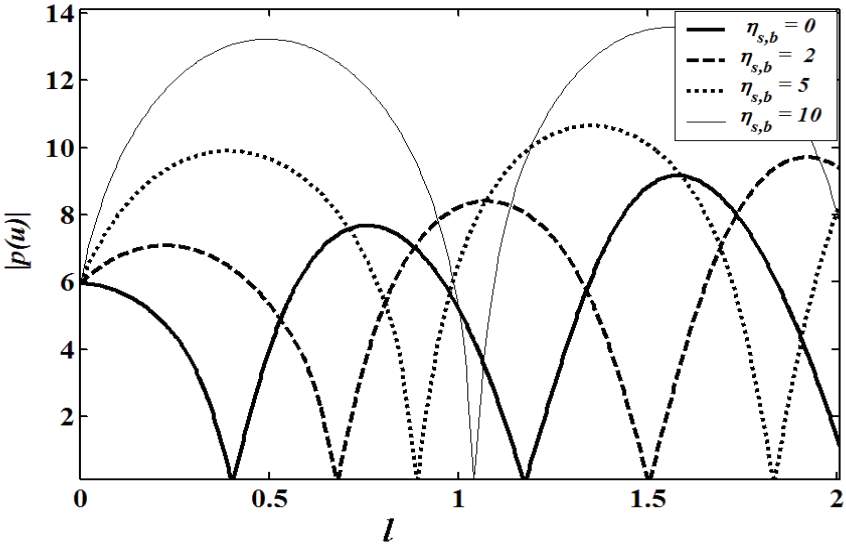

Fig. 3. Scaled polarizations $|p| = |P|/P_0$ versus scaled thickness $l = \omega_0 L/c$ for different mirror parameters $\eta_{s,b}$. Other parameters are $f = \omega/\omega_0$ = 1.1 and ε_∞ = 3.84.

bistability curves. They demonstrate the enhancement of the optical bistability due to the external feedback provided by the coating mirrors. In case $\eta_{s,b}$ = 0 (solid curves in Figs. 4) which correspond to a ferroelectric slab, the curves do not show any bistability and the response is essentially linear. In this case, it seems that the intrinsic feedback mechanism is insufficient to generate a bistable behavior. The rest of the curves illustrate that for each value of mirror parameter $\eta_{s,b}$, the bistability in $|p|$, **R**, and **T** is extended over the same range of $|e_0|$. Further, as the mirror reflectivity increases, the bistable behavior becomes more pronounced. For example at $\eta_{s,b} = 0.1$, (the dashed-curves in Figs. 4) the bistability is barely noticeable, it extends over the range $|e_0| \simeq 5204$ to $|e_0| \simeq 5227$. At $\eta_{s,b} = 0.2$, (the dotted-curves in Figs. 4) the bistability is more noticeable and its range is shifted to much lower values of $|e_0|$, where it extends over the range $|e_0| \simeq 5038$ to $|e_0| \simeq 5120$. At $\eta_{s,b} = 0.5$, (the -o- curves in Figs. 4), a wider range of optical bistability is obtained, which begins at $|e_0| \simeq 4720$ and ends at $|e_0| \simeq 4910$. Finally, at $\eta_{s,b} = 1$, (the -□- curves in Figs. 4), the bistability range is shifted to even lower values of $|e_0|$, ranging from 4535 and end at 4725. This certainly suggests that the bistability operation is improved upon increasing the mirror reflectivity. However, from the experimental point of view some important factors should be taken care of, first, the mirror material should be chosen in such a way it does not react chemically with the nonlinear medium. Second, crystal surface should be parallel to the mirror surface which requires careful alignment. Third the operating frequency should not be very close to resonance to avoid highly-absorption rates of the crystal. Unfortunately, we are unable to generate graphs for higher values of $\eta_{s,b}$ due to numerical instability. However, the curves here are sufficient to show the relationship between the optical bistability and mirror reflectivity.

Next is to draw the attention to the relationship between the bistability in the polarization *p* and reflectance **R** or transmittance **T**. Observation of these graphs shows that the bistability in **R** (Fig. 4(b)) is basically a manifestation of the bistability in $|p_t|$ (Fig. 4(a)) while the bistability in **T** (Fig. 4(d)) is a manifestation to the bistability in $|p_b|$ (Fig. 4(c)). This is explained by equations (17) and (20) where reflectance **R** and transmittance **T** are basically a function of the polarization and other material parameters. Further, the optical bistability in the macroscopic polarizarion is in fact due to the optical bistability in the microscopic polarization where the individual molecules responds nonlinearly to the driving field (Goldstone and Garmire 1984, Ibrahim and Osman 2008). In fact, this is where the advantage of Maxwell-Duffing approach is affirmed over the standard analysis in nonlinear optics, the ability to model both intrinsic and extrinsic optical bistability in one approach.

Finally, curves in Figs. 4 suggest that the threshold value of $|e_0|$ for bistability is significantly reduced by increasing mirror parameter or equivalently the mirror reflectivity. For $\eta_{s,b} = 0.1$, (the dashed-curves in Figs. 4), the threshold value of the optical bistability occurs at $|e_0|_{th} \simeq 5204$, and, for $\eta_{s,b} = 0.2$, (the dotted-curves in Figs. 4) the optical bistability starts at $|e_0|_{th} \simeq 5038$. For $\eta_{s,b} = 0.5$, (the -o- curves in Figs. 4), the optical bistability starts at $|e_0|_{th} \simeq 4720$ and for $\eta_{s,b} = 1$, (the -□- curves in all Figs. 4), the optical bistability begins at $|e_0|_{th} \simeq 4535$. Therefore, a systematic decrease of the threshold value of the driving field $|e_0|_{th}$ required for optical bistability is obtained upon increasing the mirror parameter $\eta_{s,b}$ or the mirror reflectivity.

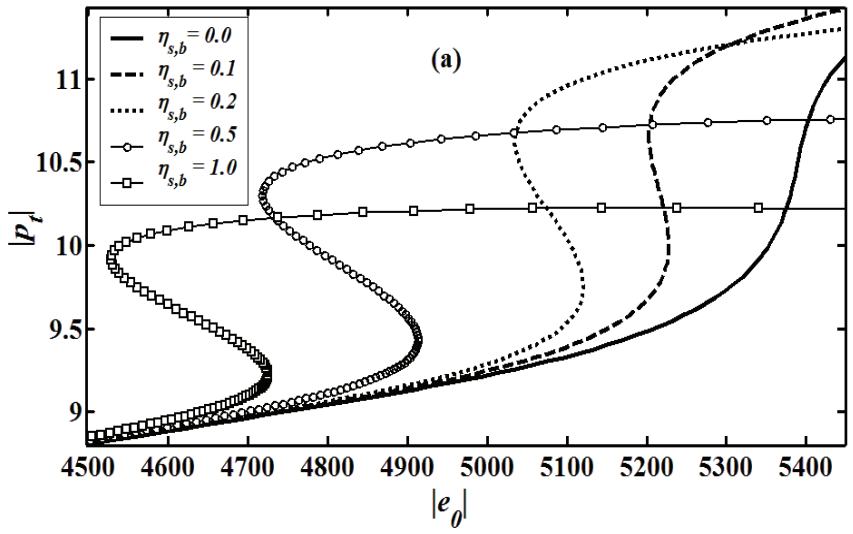

Fig. 4.(a) Polarization $|p_t| = |P_t|/P_s$ at top boundary versus electric field incident amplitude $|e_0| = E_0/E_c$ for different mirror parameters $\eta_{s,b}$ = 0, 0.1, 0.2, 0.5 and 1 corresponds to mirror reflectivity R_M = 0.127, 0.128, 0.13, 0.15 and 0.2. Other parameters are $f = \omega/\omega_0 = 1.1$, $l = \omega_0 L/c = 1.9$, $\varepsilon_\infty = 3.84$ with $t = T/T_c$ evaluated at room temperature.

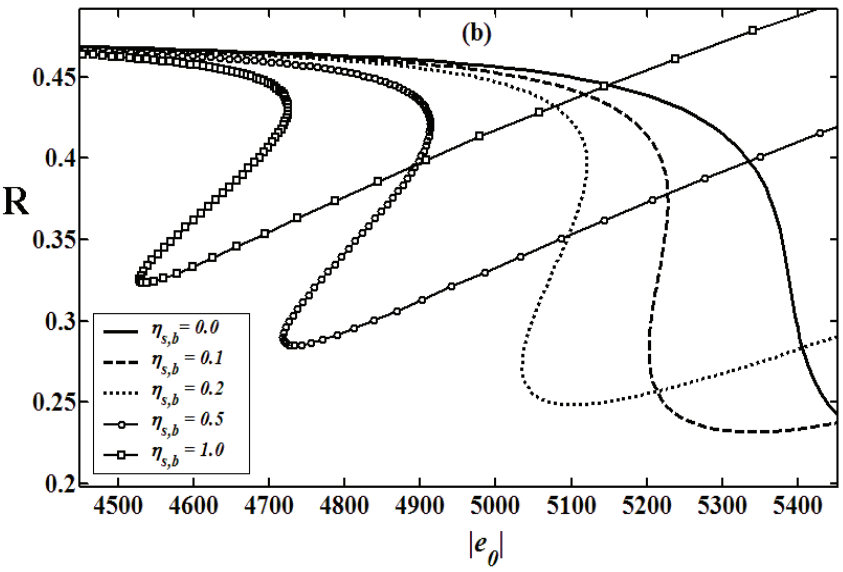

Fig. 4.(b) Reflectance $R = |r|^2$ versus $|e_0|$ for different mirror parameters. Other parameters remain as in Fig. 4(a)

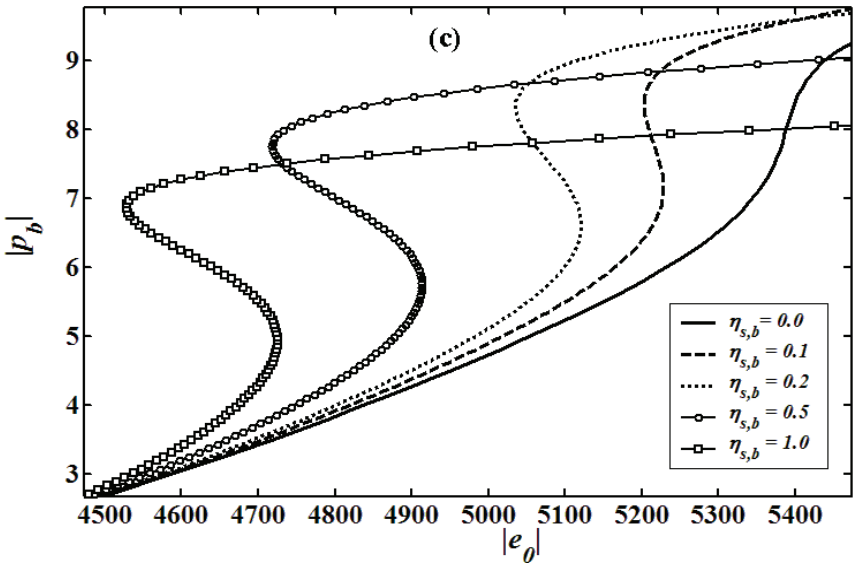

Fig . 4.(c) Polarization $|p_b| = |P_b|/P_s$ at bottom boundary $u = -\omega_0 L/c = -1$ versus electric field incident amplitude $|e_0| = E_0/E_c$ for different mirror parameters $\eta_{s,b}$ as on Fig. 4(a). Other parameters remain as in Fig. 4(a).

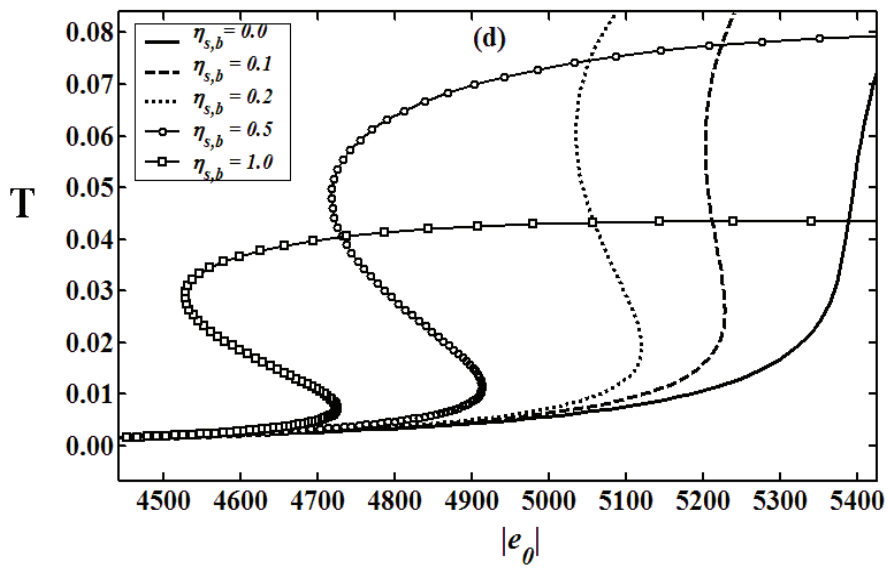

Fig. 4.(d) Transmittance $T = |\tau|^2$ versus electric field incident amplitude $|e_0| = E_0/E_c$ for different mirror parameters as in Fig. 4(a). Other parameters remain as in Fig. 4(a)

An increment in the mirror reflectivity seems to have its effect on both **R** and **T**, the switching "on" and "off" values. Observation of Fig. 4(b) shows that, for $\eta_{s,b} = 0.1$, (the dashed-curve), the reflectance switches between $\boldsymbol{R}_{off} \approx 0.27$ "off state" and $\boldsymbol{R}_{on} \approx 0.45$ "on state". For $\eta_{s,b} = 1$, (the -□- curve), the **R** "off" state increases up to $\boldsymbol{R}_{off} \approx 0.32$ while the "on" state remains at $\boldsymbol{R}_{on} \approx 0.45$. Similar behavior of transmittance **T** is also noticed in Fig. 4(d), while the "off" state remains at nearly $\boldsymbol{T}_{off} \approx 0$, the "on" state decreases gradually with increasing $\eta_{s,b}$. This is an ideal optical switch switches between "1" and "0" as the "on" and "off" state. Therefore, a better bistable operation seems to be a trade-off between mirror reflectivity and other material parameters. In other words, even a highly-reflective mirror may decrease the threshold value of the optical bistability and yet it may decrease the quality of the device as an optical switch.

It is also observed that, the nonlinear response of the system exists only for a certain range of input intensity $|e_0|$. Interestingly, the system's response to the driving field becomes linear again above this range. For example, for $\eta_{s,b} = 1$, the optical bistability starts at $|e_0|_{th} \simeq 4535$, below that threshold value of $|e_0|_{th}$ the system response is linear, and then the system starts a bistable period up to $|e_0|_{final} \simeq 4725$, beyond this value, it responds linearly to the driving field again. We have found that obtaining one bistable period through variation of ..over a wide range is basically due to a choice of relatively thin sample ($l = \omega_0 L/c = 1.9$). Increasing the thickness usually results in multistability as will be explained in the next section. It should be noted that a much higher values of the driving field $|e_0|$ from the laser source is not advisable since it may result in a material breakdown.

8. Effect of frequency

In Figs. 5, the reflectance **R** and transmittance **T** versus electric field incident amplitude $|e_0| = E_0/E_c$ are plotted for different operating frequencies $f = \omega/\omega_0$ at room temperature. Other parameters are fixed at $l = \omega_0 L/c = 3$, $\eta_{s,b} = 0$ and $\varepsilon_\infty = 3.84$. Two important features occur as the result of changing the operating frequency $f = \omega/\omega_0$. First is the change of the threshold value of the electric field incident amplitude required for optical bistability. Second is the change in the switching amplitude (the "on" and "off" state). Observation of Fig. 5(a) shows that, far above the resonance $(f = 3$ or $f \gg 1)$, the threshold value of optical bistability is $|e_0|_{th} \approx 5.87 \times 10^4$. In this case, the reflectance (curve ***i***) switches between $\mathbf{R}_{on} \approx 0.55$ and $\mathbf{R}_{off} \approx 0.08$ while the transmittance (curve ***ii***) switches between $\mathbf{T}_{on} \approx 0.8$ and $\mathbf{T}_{off} \approx 0.15$. Observation of Fig. 5(b) shows that, slightly above the resonance $(f = 1.4$ or $f > 1)$, the threshold value of optical bistability is $|e_0|_{th} \approx 1.85 \times 10^4$. In this case, the reflectance (curve ***i***) switches between $\mathbf{R}_{on} \approx 0.61$ and $\mathbf{R}_{off} \approx 0.05$ while the transmittance (curve ***ii***) switches between $\mathbf{T}_{on} \approx 0.9$ and $\mathbf{T}_{off} \approx 0.1$. Therefore, a comparison between Fig. 5(a) and Fig. 5(b) shows that at $f = 1.4$, a better switching in **T** as well as a lower threshold value is obtained comparing to the case of $f = 3$.

At resonance $(f = 1)$, observation of Fig. 5(c) shows that, the threshold value of the optical bistability is $|e_0|_{th} \approx 5.6 \times 10^3$. Two points are worth noted. First, the bistabile response is possible even at resonance where absorption in the FE material is the highest. Secondly, the threshold value of $|e_0|$ needed to induce bistability is much lower. However, even the optical bistability in reflectance is still noticeable; the transmittance in this case is practically

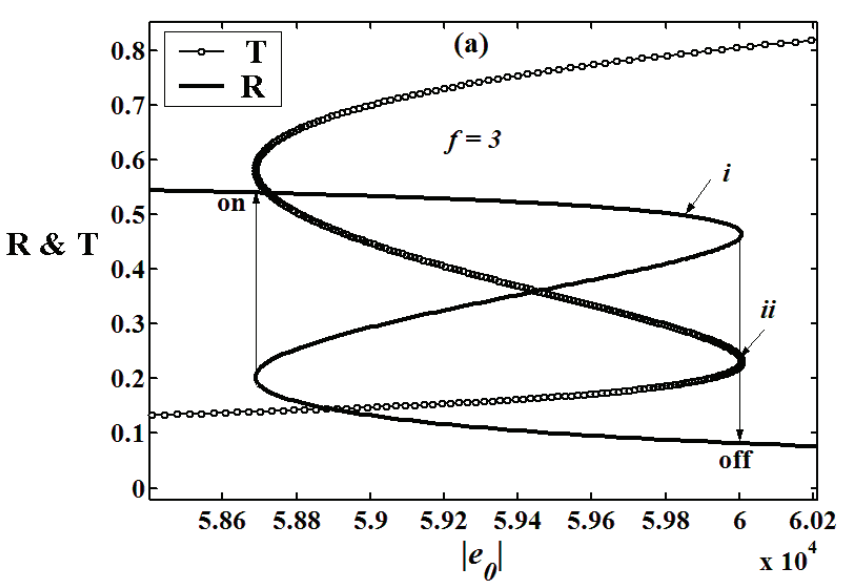

Fig. 5.(a). Reflectance R and transmittance T versus electric field incident amplitude $|e_0| = E_0/E_c$ at frequency $f = 3$. Other parameters are fixed at thickness $l = \omega_0 L/c = 1$, mirror parameter $\eta_{s,b} = 0$ and $\varepsilon_\infty = 3.84$.

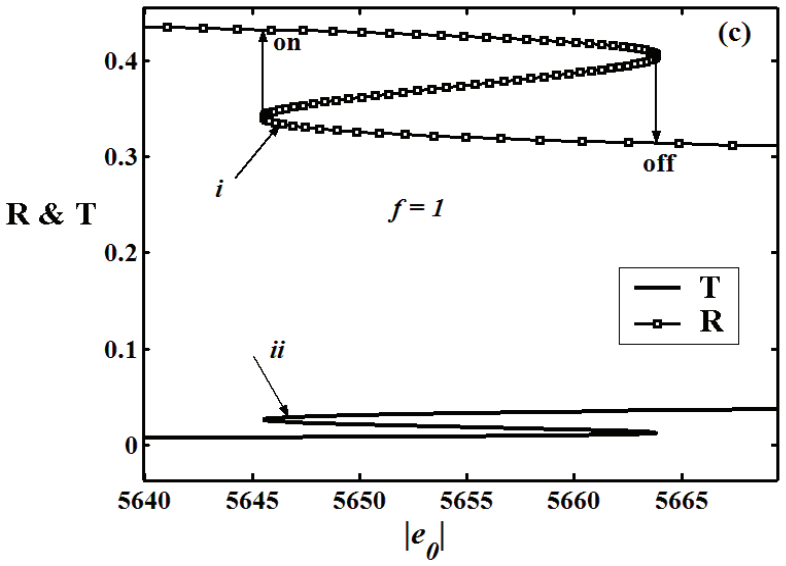

Fig. 5.(b). Reflectance R and transmittance T versus electric field incident amplitude $|e_0| = E_0/E_c$ at frequency $f = 1$. Other parameters remain as in Fig. 5(a).

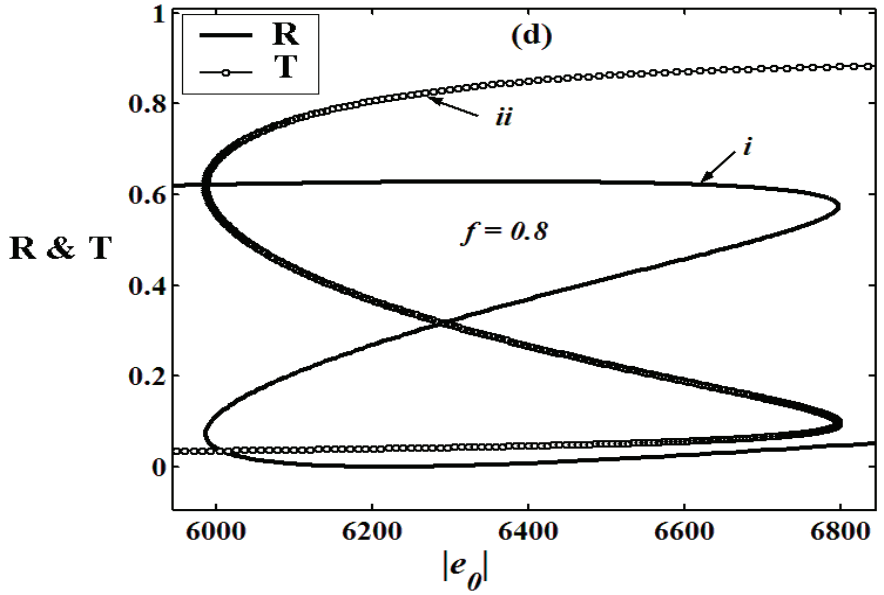

Fig. 5(c). Reflectance R and transmittance T versus electric field incident amplitude $|e_0| = E_0/E_c$ at frequency f = 0.8. Other parameters remain as in Fig. 5(a)

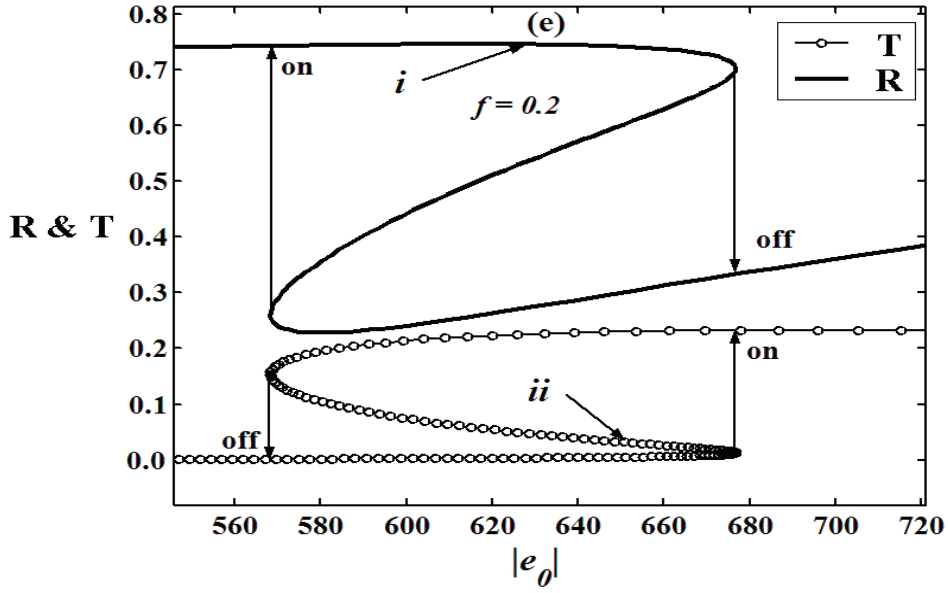

Fig. 5(d). Reflectance R and transmittance T versus electric field incident amplitude $|e_0| = E_0/E_c$ at frequency f = 0.2. Other parameters remain as in Fig. 5(a)

zero. Observation of Fig. 5(d) shows that, slightly below the resonance $(f = 0.8$ or $f < 1)$, the threshold value of optical bistability is $|e_0|_{th} \approx 6 \times 10^3$. In this case, the reflectance (curve ***i***) switches between $\mathbf{R}_{on} \approx 0.61$ and $\mathbf{R}_{off} \approx 0.02$ while the transmittance (curve ***ii***) switches between $\mathbf{T}_{on} \approx 0.88$ and $\mathbf{T}_{off} \approx 0.02$. Fig. 5(e) shows that, far below the resonance $(f = 0.2$ or $f \ll 1)$, the threshold value of optical bistability is the lowest $(|e_0|_{th} \approx 570)$. In this case, the reflectance (curve ***i***) switches between $\mathbf{R}_{on} \approx 0.74$ and $\mathbf{R}_{off} \approx 0.36$ while the transmittance (curve ***ii***) switches between $\mathbf{T}_{on} \approx 0.22$ and $\mathbf{T}_{off} \approx 0$. This means, even the threshold value of bistability is dramatically decreased, yet there is a decrease on the switching contrast between the "on" and "off" states of the switching.

Therefore, in general, the main features of bistability curves above the resonance $(f > 1)$ are found to be similar to those below the resonance $(f < 1)$ and a better bistability is obtained when the operating frequency approaches the resonance of the material from below or above. The enhancment of the optical bistability near resonance can be explained as a result of increasing the magnetude of certain tensor elements of the third-order dielectric susceptibility in this region. On the other hand, the reason for nearly zero transmittance at the exact resonance (curve ***i*** in Fig. 5(c)) may be viewed as a result of rapid depletion of incident optical pump wave or the newly generated signal wave (He 2000). Therefore, the proper choice of the operating frequency is a compromise between the enhancement of the nonlinear susceptibility and the attenuation of the useful optical wave. For this reason, an operating frequency in a quasi-resonance is often employed by tuning the frequency of the incident laser beam to be close but not equal to the resonance of the medium. The threshold value of the optical bistability decreases in general with decreasing *f*. However, from our calculated curves for a larger range of frequencies, some variation in the threshold values are found. For example, the threshold value of $|e_0|$ at $f = 0.8$ is slightly higher than that of $|e_0|$ at $f = 1$ as seen from Fig. 5.7(c) and Fig. 5.7(d). This is may be due to the variation in detuning but the main effect remains.

9. Conclusion

The Maxwell-Duffing analysis has been employed to study the optical bistability of a ferroelectric slab as well as a Fabry-Perot resonator coated with two identical partially-reflecting dielectric mirrors. The nonlinear response of the polarization *P* to an optical driving field *E* using the Landau-Khalatnikov dynamical equation has been modeled. The Landau-Devonshire free energy expression for bulk FE material assumed to exhibit a second-order phase transition has been utilized. Using single frequency approximation and assuming normal incidence, the driving field in the LK equation is substituted into the electromagnetic wave equation to produce a nonlinear polarization equation. For convenience in numerical simulation, all variables are converted into dimensionless form. The resulting nonlinear polarization equation is numerically integrated across the thickness of the FE medium. With the application of the exact nonlinear boundary conditions, expressions for both reflectance *R* and transmittance **T** are derived as a function of the total polarization *p*, electric field incident amplitude $|e_0|$, and other material parameters such as temperature. The behaviors of the polarization at top and bottom interface, reflectance **R**, and transmittance **T** have been plotted versus electric field incident amplitude $|e_0|$. The

effects of mirror parameter η_s, and frequency f on the optical bistability have been investigated. The input parameters used in this simulation are based on available experimental data of $BaTiO_3$.

It is found that the system responds linearly to the driving field at relatively low electric field incident amplitude $|e_0|$. After $|e_0|$ exceeds certain threshold value, the response becomes nonlinear. The threshold value of the bistability phenomenon was found to have a function of mirror reflectivity R_M, and operating frequency f. The bi-stability in both reflectance and transmittance has been demonstrated which is a manifestation of the bistability in the polarization itself. The bistability in the macroscopic polarization is proportional to the bistability in the microscopic domain. The current approach is more suitable for ferroelectrics particularly at frequency ranges where the nonlinear response of the material is strong and resonant. The intrinsic optical bistability obtained is in agreement with the experimental results of intrinsic optical bistability obtained recently for $BaTiO_3$ (Ciolek 2006).

This method could be applied to oblique incidence and to multilayers. Apart from the considerable difference between this approach and the standard approach in nonlinear optics, the graphs shown are qualitatively similar to those found in the textbook analysis. It might also be possible to study the behavior of this system without the use of single frequency approximation to examine the characteristics of the full dynamic in time domain which may lead to chaos.

10. Refrences

Biran B., Opt. Commun. 74 183 (1990).

Born M. and Wolf E., Principles of Optics, "*Electromagnetic Theory of vPropagation, Interference and Diffraction of Light*", 6th ed. Pergamon, Oxford, (1980).

Cao W., and Cross L.E., Phys. Rev. B 47 4285 (1993).

Chew K-H, Osman J. and Tilley D. R., Opt. Commun. 191, 393 (2001).

Ciolek R., Osuch K., Pura B., Wierzbicki M., Zagórski A., and Wrzesiński Z., Optical Materials 28, 1341 (2006).

Danckaert J., Thienpont H., Vertennicofff I., Haelterman M., and Mandel P., Opt. Commun. 71 317 (1989).

Dawber M., Rabe K. M., and Scott J. F., Reviews of Modern Physics, 77, 1083 (2005).

Dormand, J. R. and Prince P. J., *J. Comp. Appl. Math.* 6 19 (1980).

Eaton D. F., Science, New Series, Vol. 253, No. 5017, 281 (1991).

Fatuzzo E., and Merz W. J., *Ferroelectricity*. North-Holland Publishing Co, Amsterdam: (1967).

Feng, S.H. and J.S. Chen, *Frontiers of solid state chemistry: proceedings of the International Symposium on Solid State Chemistry in China, Changchun, China,* (2002).

Gibbs H.M., McCall S.L., and Venkatesan T.N.C.: Optical bistability. Optics News, 6 (1977).

Gibbs, H. M., McCall, S. L., Venkatesan T. N. C., Gossard A. C., Passner A., and Wiegmann W., *Appl. Phys. Lett.* 35, 451(1979).

Gibbs H.M. "*Optical bistability*: *controlling light with light*", Academic Press, Inc., Orlando FL, (1985)

Ginzburg V. L. "Phase Transitions and Critical Phenomena", In *Ferroelectricity: The Fundamentals Collection,* Gonzalo J. A., and Jiménez B., WILEY- VCH Verlag GmbH & Co. KGaA, Weinheim (2005)

Goldstone J. A., and Garmire E., Phys. Rev. Lett. 53 910 (1984)

Gupta S., and Agrawal G. S., J. Opt. Soc. Am. B 4 691 (1987).

Haelterman M., Mandel P., Danckaert J., Thienpont H., Vertennicofff I., Opt. Commun. 74, 238 (1989).

He, G. S., and Liu S. H., "*Physics of Nonlinear Optics*", World Scientific, (2000).

Hehlen M.P., Gudel H.U., Shu Q., Rai J., Rai S., and Rand S.C., Phys. Rev. Lett. 73 1103 (1994).

Hehlen M.P., Kuditcher A., Rand S.C., and Luthi S.R., Phys. Rev. Lett. 82 3050 (1999)

Ibrahim A-B M. A., Tilley D. R., and Osman J., Ferroelectrics, 355 (1) 140 (2007)

Ibrahim, A. B. M. A., and Osman, J., *Euro. Phys. J., B* 63, 193 (2008).

Kanzig W. and Meier R., Helv. Phys. Acta 21, 585 (1949).

Lim S.-C., Osman J., and Tilley D. R., J. Phys.: Condens. Matter 9 8297 (1997).

Lines M. E., and Glass A.M., "*Principles and Applications of Ferroelectrics and Related Materials*", Clarendon Press, Oxford, (1977)

Mantese J. V., and Alpay S. P., "*Graded Ferroelectrics, Transcapacitors and Transponents*"., Springer, New York, (2005).

Marburger J. H., and Felber F.S., Phys. Rev. A. 17 335 (1978).

Merz,W . J., Phys. Rev. 76 1221 (1949)

Merz W. J., Phys. Rev. 91, 513 (1953)

Murgan R., Tilley D. R., Ishibashi Y., Webb J. F., and Osman J., J. Opt. Soc. Am. B 19 2007 (2002).

Murgan R., Razak F., Tilley D. R., Tan T. Y., Osman J., and Halif M. N. A., Computational Material Science., 30 468 (2004).

Mitsui T., Tatsuzaki I., and Nakamura E., "*An Introduction to the Physics of Ferroelectrics*", Gordon and Breach, London, (1976)

Osuch K., Pura B., Petykiewicz J., Wierzbicki M., and Wrzesiński Z., Optical Materials 27, 39 (2004).

Przedmojski J., and Pura B., Ferroelectrics 21, 545 (1978).

Pura B., Jda W., Noniewicz K., and Zagórski A., J. Nonlinear Opt. Phys. Mater. 7 441 (1998)

Rabe K. M., Ahn C. H., and Triscone J-M., "*Physics of ferroelectrics: a modern perspective*", Springer, Berlin, (2007)

Ramesh R. Aggarwal S. and Auciello O., Materials Science and engineering 32 (2001).

Seitz F., and Turnbull D., "*Solid State Physics. Advances in research and application*", vol. 4, Academic Press, New York, (1957).

Shen Y. R., *The Principles of Nonlinear Optics*, Wiley, New York, (1984).

Shi F.W. , Meng X.J., Wang G.S., Sun J.L., Lin T., Ma J.H., Li Y.W., and Chu J.H., Thin Solid Films 496 333 (2006)

Snieder R., "*A guided tour of mathematical methods for the physical sciences*", 2nd ed., Cambridge University Press (2004)

Sutherland R. L, "*Handbook of Nonlinear Optics*", Marcel Dekker Inc, New York: (1996).
Xuan L., Pan S., Chen Z., Wang R., Shi W., and Li C., Appl. Phys. Lett. 73 2896 (1998).
Zhang S., Dong X., and Kojima S.. Jpn. J. Appl. Phys. 36 2994 (1997).
Zhao Q., Liu Y., Shi W., Ren W., Zhang L., and Yao X., Appl. Phys. Lett. 69 458 (1996).

Ferroelectrics

Edited by Dr Indrani Coondoo

ISBN 978-953-307-439-9
Hard cover, 450 pages
Publisher InTech
Published online 14, December, 2010
Published in print edition December, 2010

Ferroelectric materials exhibit a wide spectrum of functional properties, including switchable polarization, piezoelectricity, high non-linear optical activity, pyroelectricity, and non-linear dielectric behaviour. These properties are crucial for application in electronic devices such as sensors, microactuators, infrared detectors, microwave phase filters and, non-volatile memories. This unique combination of properties of ferroelectric materials has attracted researchers and engineers for a long time. This book reviews a wide range of diverse topics related to the phenomenon of ferroelectricity (in the bulk as well as thin film form) and provides a forum for scientists, engineers, and students working in this field. The present book containing 24 chapters is a result of contributions of experts from international scientific community working in different aspects of ferroelectricity related to experimental and theoretical work aimed at the understanding of ferroelectricity and their utilization in devices. It provides an up-to-date insightful coverage to the recent advances in the synthesis, characterization, functional properties and potential device applications in specialized areas.

How to reference

In order to correctly reference this scholarly work, feel free to copy and paste the following:

Abdel-baset Ibrahim, Mohd Kamil Abd Rahman and Junaidah Osman (2010). Ferroelectric Optics: Optical Bistability in Nonlinear Kerr Ferroelectric Materials, Ferroelectrics, Dr Indrani Coondoo (Ed.), ISBN: 978-953-307-439-9, InTech, Available from: http://www.intechopen.com/books/ferroelectrics/ferroelectric-optics-optical-bistability-in-nonlinear-kerr-ferroelectric-materials-

INTECH
open science | open minds

InTech Europe
University Campus STeP Ri
Slavka Krautzeka 83/A
51000 Rijeka, Croatia
Phone: +385 (51) 770 447
Fax: +385 (51) 686 166
www.intechopen.com

InTech China
Unit 405, Office Block, Hotel Equatorial Shanghai
No.65, Yan An Road (West), Shanghai, 200040, China
中国上海市延安西路65号上海国际贵都大饭店办公楼405单元
Phone: +86-21-62489820
Fax: +86-21-62489821